

Can UV light fight coronavirus?

Ultraviolet light can kill the novel coronavirus – COVID-19

According to the latest guideline on the diagnosis and treatment of the novel coronavirus released by the National Health Commission, the virus is sensitive to ultraviolet light and heat, so ultraviolet radiation can effectively eliminate the virus.

<https://www.khmertimeskh.com/50701725/ultraviolet-light-can-kill-the-novel-coronavirus-covid-19/>

<https://www.chinadaily.com.cn/a/202003/04/WS5e5ee878a31012821727c0f4.html>



What kills novel coronavirus?

Updated: 2020-03-18 | chinadaily.com.cn



In the seventh guideline on the diagnosis and treatment of the novel coronavirus released by the National Health Commission, several substances are listed as effective ways to inactivate the coronavirus. Let's have a careful check and listen to its advice.

1. Ultraviolet light

The novel coronavirus is sensitive to ultraviolet light, so ultraviolet radiation can effectively eliminate the virus.

Ian Lipkin, director of the Columbia University's Center for Infection and Immunity, has been studying the novel coronavirus. He says sunlight, which is less abundant in winter, can also help break down viruses that have been transmitted to surfaces.

“UV light breaks down nucleic acid. It almost sterilizes [surfaces]. If you’re outside, it’s generally cleaner than inside simply because of that UV light,” he says.

UV light is so effective at killing bacteria and viruses it’s often used in hospitals to sterilize equipment.

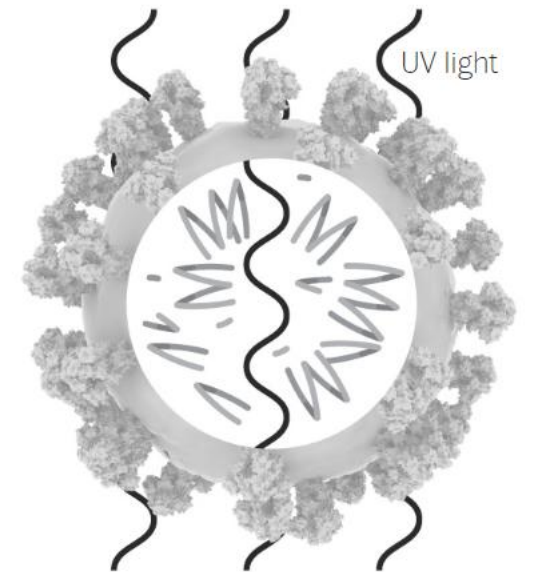
How UV light fight coronavirus?

For several decades, it has been known by scientists that broad-spectrum germicidal UV light, with wavelengths between 200 and 400 nanometers (nm), is very effective at killing bacteria and viruses by destroying bonds that hold their DNA together.

In addition, oxygen can also absorb energy from UV light to form ozone for disinfection. Ultraviolet light UV-C not only kills the virus on surfaces, but also those in the air.

The novel coronavirus is a kind of positive-sense single-stranded RNV virus, same as the SARS and MERS virus. Researches on SARS found that this kind of virus is sensitive to heat radiation and UVC light and can be diminished when exposure to UVC irradiation stronger than $90 \mu\text{W}/\text{cm}^2$.

Ultraviolet light disrupts the genetic material.



Synthesis of Coronavirus mRNAs: Kinetics of Inactivation of Infectious Bronchitis Virus RNA Synthesis by UV Light

DAVID F. STERN^{1,2*} AND BARTHOLOMEW M. SEFTON²

¹Department of Biology, University of California, San Diego, La Jolla, California 92093, and ²Tumor Virology Laboratory, The Salk Institute, San Diego, California 92138²

Received 9 November 1981/Accepted 22 December 1981

Infection of cells with the avian coronavirus infectious bronchitis virus results in the synthesis of five major subgenomic RNAs. These RNAs and the viral genome form a 3' coterminal nested set. We found that the rates of inactivation of synthesis of the RNAs by UV light were different and increased with the length of the transcript. These results show that each RNA is transcribed from a unique promoter and that extensive processing of the primary transcripts probably does not occur.

The coronaviruses are enveloped viruses which cause diverse diseases (reviewed, 18). These viruses have an unusually large single-stranded RNA genome which is infectious and hence of positive polarity (14, 21). Coronavirus genome expression appears to differ from that of other positive-stranded RNA viruses in the use of multiple overlapping subgenomic mRNAs.

Six or seven RNA species are synthesized in coronavirus-infected cells. They are likely to be viral mRNAs since they are capped (11, 11a), polyadenylated (5, 11, 24, 26), associated with polyribosomes (24, 28), and some have been translated in vitro to yield viral proteins (5, 19, 22, 25). We have shown that the avian coronavirus infectious bronchitis virus (IBV) specifies six major RNA species in infected chicken embryo kidney cells (26). They consist of the genome (RNA F) and five subgenomic RNAs which range in size from 0.8×10^6 to 2.6×10^6 daltons (Table 1). We have designated the subgenomic RNAs A, B, C, D, and E, with RNA A being the smallest and RNA E the largest. RNase T₁ oligonucleotide fingerprint analysis of these RNAs showed that each RNA contained all of the oligonucleotides found in every smaller RNA plus additional ones (26, 27). The RNAs thus comprise a nested set. The subgenomic RNAs were mapped relative to the genome by comparing their oligonucleotide maps with maps obtained from defined portions of the genome. This showed that the subgenomic RNAs are colinear with the genome and that they correspond to 3' terminal portions of the genome (27). Each RNA differs from the next smaller species in its inclusion of additional 5' terminal sequences. T₁ RNase fingerprinting of intracellular RNAs specified by murine coronaviruses A59 and JHM produced similar results (11, 13). Support for this conclusion was obtained by

using a different approach with mouse hepatitis virus A59. Complementary DNA was synthesized by reverse transcription of the smallest intracellular virus-specific RNA and was found to hybridize to all of the subgenomic RNAs (5), a result expected if each includes the sequences of the smallest RNA.

Little is known about the mechanism of viral RNA synthesis in coronavirus-infected cells. The viruses replicate in the cytoplasm of infected cells, and it is likely that no primary nuclear function is required since coronaviruses can multiply in enucleated cells (30). There is no evidence for differential temporal regulation of the synthesis of the RNAs. The intracellular RNAs are not, however, equally abundant (13, 26), and their accumulation must therefore be regulated, possibly at the transcriptional level.

The synthesis of the coronavirus mRNAs could occur by two rather different mechanisms. First, a single primary transcript could be processed to yield the subgenomic RNAs by removal of 5' terminal sequences. Alternatively, there could be a unique promoter for the transcription of each RNA. It should be possible to distinguish these mechanisms by measuring the kinetics with which synthesis of the mRNAs is inactivated by UV light. This approach has been used for transcriptional studies of several viruses in which mRNAs are transcribed from RNA templates (1, 2, 4, 8, 9). The technique is based upon the chain-terminating effects of UV photoproducts in the template (reviewed, 20). Potential sites for these lesions are distributed randomly along the templates, and one lesion is sufficient to terminate transcription. Thus, inactivation of templates by UV light occurs with pseudo-first-order kinetics, which is described by the expression $\ln N/N_0 = -kd$ in which N is the number of active templates and N_0/N_0 is the fraction of

TABLE 1. UV target sizes calculated from the experiment in Fig. 2

RNA	Slope of inactivation curve ^a	Estimated target size $\times 10^{-6}$ daltons ^b	Physical size of transcript $\times 10^{-6}$ daltons ^c
A	-0.1028	(12)	0.8
B	-0.1263	0.97 (12)	0.9
C	-0.2084	1.6 (12)	1.3
D	-0.1824	1.4 (12)	1.5
E	-0.4186	3.2 (11)	2.6
F	-0.6385	5.2 (11)	(6.9)

^a Slopes of the inactivation curves were determined by linear regression analysis of data from the legend to Fig. 1, as described in the legend to Fig. 2.

^b UV target sizes were calculated from the slopes, with the assumption that the physical target size for synthesis of RNA A is equal to the size of RNA A as follows:

$$\text{target size}_{\text{RNA Z}} = \text{slope}_Z \times \frac{\text{target size}_{\text{RNA A}}}{\text{slope}_A}$$

$$= \text{slope}_Z \times \frac{0.8 \times 10^6 \text{ daltons}}{-0.1028}$$

The number of datum points analyzed is indicated in parentheses.

^c From reference 26.

templates remaining active at UV dose d ; k is the inactivation cross-section, or target size. If the coronavirus mRNAs are produced by processing of a single precursor, the synthesis of every RNA would be equally sensitive to UV light. However, if each RNA is transcribed by initiation at a unique site then the transcriptional target size should differ for each transcript.

We have used this approach to examine the mechanism of synthesis of the IBV mRNAs. We found that the UV target size for synthesis of each RNA was different and increased with the size of the transcript. These results are consistent with a model wherein each RNA species is transcribed from a unique promoter, and no major nucleolytic processing occurs. Similar results were recently reported by Jacobs et al. for UV transcriptional mapping with the murine coronavirus A59 (9).

The experimental protocol was as follows. Parallel cultures of IBV-infected chicken embryo kidney cells were irradiated with UV light and then incubated for 90 min with [³²P]orthophosphate to label transcripts synthesized on the remaining templates. This incubation was carried out in the presence of actinomycin D to inhibit transcription of host cell DNA and cycloheximide and to reduce the synthesis of new templates by preventing the synthesis of polymerase molecules. Cytoplasmic RNA was ex-

tracted, denatured with glyoxal, and analyzed on agarose slab gels. The synthesis of each intracellular RNA species was quantified by measuring the radioactivity in bands excised from the gels or by densitometry of the autoradiographs.

It was necessary to analyze equivalent amounts of RNA from each culture to permit a quantitative comparison among different gel tracks. Two potential sources of variability were the inevitable heterogeneity of the chicken embryo kidney cell cultures and the possibility of losses during the RNA extractions. The problem was partly circumvented by prelabeling the cells with [³H]uridine for 12 h before infection and adjusting the gel samples so that equivalent ³H-labeled activity was applied in each lane. Some variation remained, however, and tracks which obviously contained disproportionate amounts of material were omitted from the analysis of the data (see below).

The autoradiograph for one transcriptional inactivation experiment (experiment 4) is shown in Fig. 1. Synthesis of the genome (RNA F) dropped rapidly with increasing UV doses, but the small RNAs A and B were relatively resistant (compare Fig. 1, lanes a and g). In other experiments, greater UV doses were employed to obtain more complete inactivation of synthesis of the smaller RNAs. Lane e was excluded from further analysis because it evidently contained substantially more RNA than the non-irradiated controls (lanes a, b, and c). The data in Fig. 1 were quantified by densitometry, and the results are plotted in Fig. 2. Lines were fitted to the inactivation curves by linear regression, and the slopes for these lines are listed in Table 1.

The inactivation curves of the RNAs were quite different. This rules out the possibility that the RNAs were synthesized by processing of a single precursor. We calculated transcriptional target sizes for RNAs B, C, D, E, and F, with the assumption that the template region encoding RNA A is equal in size to RNA A (Table 1). The transcriptional target sizes were in approximate agreement with the sizes of the transcripts determined from their electrophoretic mobilities (Table 1). Target sizes calculated in the same way from four transcriptional inactivation experiments are shown in Table 2. In all four experiments there was a direct relationship between the size of the transcript and the corresponding target size.

The resolution of the experiments was apparently not sufficient to distinguish between the target sizes for inactivation of synthesis of RNA A and RNA B or between RNA C and RNA D. These RNAs differ in size by only 10%. Some of the calculated inactivation curves deviated from

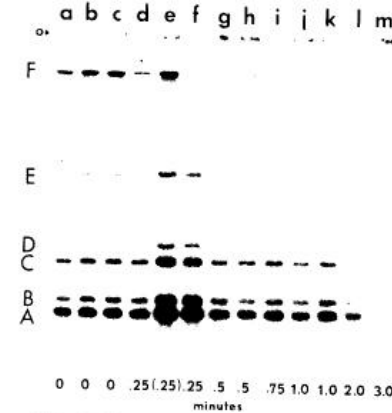


FIG. 1. Effect of UV irradiation on IBV RNA synthesis (experiment 4). Chicken embryo kidney cells prepared as described previously (26) were seeded in 6-cm culture dishes in 4 ml of Dulbecco modified Eagle medium containing 10% heat-inactivated horse serum. Twelve hours before infection, 50 μ Ci of [5,6-³H]uridine (37.6 Ci/mmol, New England Nuclear Corp.) was added to each culture. Cells were washed with Tris-buffered saline and infected with IBV (Beaudette strain) at a multiplicity of infection of 20 PFU per cell. After incubation for 90 min at 38°C, the inoculum was replaced with 4 ml of Dulbecco modified Eagle medium containing 1/10th the usual amount of phosphate and supplemented with 1% calf serum (dialyzed against 160 mM NaCl) and 1 μ g of actinomycin D per ml (a gift from Merck Sharpe & Dohme). After 5.5 h, the cultures were washed once with Tris-buffered saline containing 1% dialyzed calf serum. Two milliliters of the same buffer was added to each culture, and experimental cultures were irradiated with a General Electric G4T4.1 lamp at a distance of 25 cm. The intensity of UV light was approximately 380 μ W/cm²; exposure times ranged from 0.25 to 6 min. The plates were then incubated for an additional 1.5 h in 2.0 ml of phosphate-free Dulbecco modified Eagle medium containing 1% dialyzed calf serum, 1 μ g of actinomycin D per ml, 10 μ g of cycloheximide per ml (Calbiochem-Boehringer), and 0.4 mCi of [³²P]orthophosphate (carrier-free, 285 Ci/mg, ICN). The plates were then washed twice with cold phosphate-buffered saline and once with TNE (50 mM Tris [pH 7.4], 100 mM NaCl, and 1 mM EDTA), and the cytoplasmic RNA was extracted as previously described (17). RNA was recovered by centrifugation, washed twice with 5 ml of 70% ethanol-50 mM NaCl, dried, and treated with glyoxal (16, 17). Two- μ l samples were spotted on DEAE filter disks (Whatman DE81, Whatman Inc.). The disks were washed three times with 5% Na₂HPO₄, once with water, and once with ethanol, dried, and the ³H activity was determined by scintillation spectrometry. Gel samples were prepared by dilution with glyoxal buffer so that each gel track was loaded with equivalent tritium activity (1.1 $\times 10^6$ cpm) in 70 μ l. Since ³H

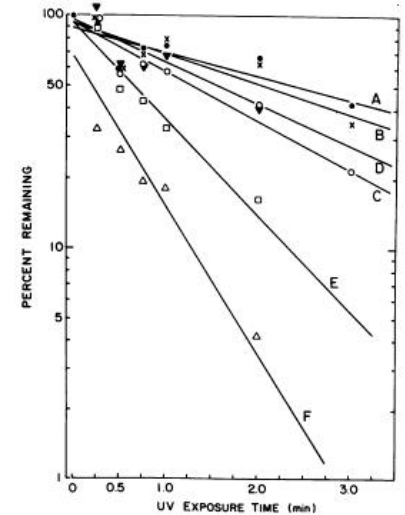


FIG. 2. Kinetics of inactivation of IBV RNA synthesis (experiment 4). The autoradiograph in Fig. 1 was scanned with a Joyce-Loebel recording microdensitometer. Areas of peaks corresponding to each RNA were determined with a Hewlett-Packard digitiser. RNA synthesis, expressed as a percentage of the geometric mean values obtained for the same RNA species in the non-irradiated cultures (Fig. 1, lanes a, b, and c), is plotted along the ordinate and UV light exposure times on the abscissa. The data in Fig. 1, lane e, were not included for reasons discussed in the text. Inactivation curves were fitted to the datum points by linear regression. Each point was considered separately for this analysis, but average values for each exposure time are shown in the figure for greater clarity. Following are symbols corresponding to UV inactivation curves for the synthesis of RNA A, \bullet ; B, \circ ; C, \square ; D, \triangle ; E, \blacksquare ; and F, \blacktriangle .

ideal first-order inactivation kinetics in that they did not intersect the origin (100% template activity with no UV exposure, see Fig. 2, RNA F). This result could indicate a greater initial rate of

activity was more than 30-fold greater than ³²P activity, spillover of ³²P to the ³H channel was insignificant. Electrophoresis in 1.2% agarose gels was as described before (17), except that the running buffer contained 0.2% sodium dodecyl sulphate. The dried gel displayed here (experiment 4) was exposed to Kodak X-Omat R film for 20 h at room temperature. "O" designates the electrophoretic origin. Intracellular RNAs A, B, C, D, E, and F are marked. UV light exposure times (in minutes) are indicated for each lane.

TABLE 2. UV target sizes calculated from four experiments

RNA	Estimated target size $\times 10^{-6}$ daltons ^a				Mean target size $\times 10^{-6}$ daltons ^b	Physical size of transcript $\times 10^{-6}$ daltons ^c
	Exp 1	Exp 2	Exp 3	Exp 4		
A	(7)	(12)	(11)	(12)		0.8
B	0.64 (8)	0.80 (12)	0.9 (11)	0.97 (12)	0.83	0.9
C	0.87 (8)	1.5 (11)	0.9 (11)	1.6 (12)	1.2	1.3
D	0.81 (8)	1.2 (10)	1.5 (9)	1.4 (12)	1.2	1.5
E	3.1 (6)	5.9 (6)	3.7 (6)	3.2 (11)	4.0	2.6
F	3.7 (6)	7.1 (6)	ND ^d	5.2 (11)	5.4	(6.9)

^a Experiments 1, 2, and 3 were performed as described in the legend to Fig. 1, except that data in experiments 1 and 2 were quantified by scintillation spectrometry of the excised gel bands and those for experiment 3 were quantified by densitometry of an indirect autoradiograph prepared with preflashed film and exposed with an intensifying screen at -70°C (12). Target sizes were determined from the slopes of inactivation curves as described in footnote *b* to Table 1. The number of datum points analyzed is indicated in parentheses.

^b Mean value for target sizes determined in experiments 1, 2, 3, and 4.

^c From reference 26.

^d ND, Not determined.

inactivation and may reflect secondary effects of UV light on transcription.

The results in Table 2 are in agreement with those obtained from similar experiments with mouse hepatitis virus A59 (9). They are most simply explained by the existence of a unique promoter for the synthesis of each RNA. Extensive processing of the primary transcript probably does not occur since there is an approximate proportionality between the UV target size for the synthesis of each RNA and the size of the final transcript. A possible exception is RNA E, for which the relative target size measured was consistently greater than that predicted from the model. No such discrepancy was found for any A59 RNA (9). There is some uncertainty about the size of RNA F, the IBV genome (6, 15, 26), because of the difficulties inherent in determining the size of a large RNA molecule. It is not clear, therefore, how closely the calculated UV target size for synthesis of the genome agrees with its physical size.

M. Lai et al. have reported that RNAs specified by A59 virus all contain the same 5' terminal oligonucleotide (11a). The results of the transcriptional inactivation experiments rule out the possibility that a common leader sequence is spliced to each RNA. The simplest explanation for the identical 5' sequences is that the shared oligonucleotide is encoded at each of the multiple transcriptional initiation sites. The identical 5' termini of the five vesicular stomatitis virus mRNAs have been found to be encoded in each viral gene (7).

The physical form of the template(s) for coronavirus mRNA synthesis is unknown. The subgenomic mRNAs could be transcribed by internal initiation on a genome-length template, or there might be separate templates for the synthesis of each RNA. The mechanism of synthesis of the two alphavirus mRNAs may be

analogous to that involved in the synthesis of the coronavirus mRNAs. One of the alphavirus mRNAs is the 42S viral genome. The other mRNA corresponds to the 3' terminal portion of the genome and thus resembles each coronavirus subgenomic RNA in its relationship to the genome (10, 29). It is likely that both alphavirus mRNAs are transcribed from genome-length templates since truncated negative-stranded templates have not been detected in replicative intermediates (3, 23).

The experiments reported here support the hypothesis that there is a distinct promoter for the initiation of synthesis of each coronavirus mRNA. Separate promoters have the potential to allow independent transcriptional regulation of the synthesis of each mRNA.

D. Stern was supported by Training Grant GM 07313. This work was supported by Public Health Service grants CA 14195 and CA 17289 and by Biomedical Research Support grant RR05595 from the National Institutes of Health.

LITERATURE CITED

1. Abraham, G., and A. K. Banerjee. 1976. Sequential transcription of the genes of vesicular stomatitis virus. *Proc. Natl. Acad. Sci. U.S.A.* 73:1504-1508.
2. Ball, L. A., and C. N. White. 1976. Order of transcription of genes of vesicular stomatitis virus. *Proc. Natl. Acad. Sci. U.S.A.* 73:442-446.
3. Bruton, C. J., and S. I. T. Kennedy. 1975. Semliki forest virus intracellular RNA: properties of the multi-stranded RNA species and kinetics of positive and negative strand synthesis. *J. Gen. Virol.* 28:111-127.
4. Brzeski, H., and S. I. T. Kennedy. 1978. Synthesis of alphavirus-specified RNA. *J. Virol.* 25:630-640.
5. Cheley, S., R. Anderson, M. J. Cupples, E. C. M. L. Chan, and V. L. Morris. 1981. Intracellular murine hepatitis virus-specific RNAs contain common sequences. *Virology* 112:596-604.
6. Davies, H. A., R. R. Dourmashkin, and M. R. MacNaughton. 1981. Ribonucleoprotein of avian infectious bronchitis virus. *J. Gen. Virol.* 53:67-74.
7. Gallione, C. J., J. R. Greene, L. E. Iverson, and J. K. Rose. 1981. Nucleotide sequences of the mRNAs encoding the vesicular stomatitis virus N and NS proteins. *J. Virol.* 39:529-535.
8. Glazier, K., R. Raghov, and D. W. Kingsbury. 1977.

9. Jacobs, L., W. J. M. Spaan, M. C. Horzinek, and B. A. M. van der Zeijst. 1981. Synthesis of subgenomic mRNAs of mouse hepatitis virus is initiated independently: evidence from UV transcription mapping. *J. Virol.* 39:401-406.
10. Kennedy, S. I. T. 1976. Sequence relationships between the genome and the intracellular RNA species of standard and defective-interfering Semliki Forest virus. *J. Mol. Biol.* 108:491-511.
11. Lai, M. M. C., P. R. Brayton, R. C. Armes, C. D. Patton, C. Pugh, and S. A. Stohman. 1981. Mouse hepatitis virus A59: mRNA structure and genetic localization of the sequence divergence from hepatotropic strain MHV-3. *J. Virol.* 39:823-834.
- 11a. Lai, M. M. C., C. D. Patton, and S. A. Stohman. 1982. Further characterization of mRNA's of mouse hepatitis virus: presence of common 5'-end nucleotides. *J. Virol.* 41:557-565.
12. Laskey, R. A., and A. D. Mills. 1977. Enhanced autoradiographic detection of ^{32}P and ^{35}S using intensifying screens and hypersensitive film. *FEBS Lett.* 82:314-316.
13. Leibowitz, J. L., K. C. Wilhelmson, and C. W. Bond. 1981. The virus-specific intracellular RNA species of two murine coronaviruses: MHV-A59 and MHV-JHM. *Virology* 114:39-51.
14. Lomniczi, B. 1977. Biological properties of avian coronavirus RNA. *J. Gen. Virol.* 36:531-533.
15. Lomniczi, B., and I. Kennedy. 1977. Genome of infectious bronchitis virus. *J. Virol.* 24:99-107.
16. McMaster, G. K., and G. G. Carmichael. 1977. Analysis of single- and double-stranded nucleic acid on polyacrylamide and agarose gels by using glyoxal and acridine orange. *Proc. Natl. Acad. Sci. U.S.A.* 74:4835-4838.
17. Meinkoth, J., and S. I. T. Kennedy. 1980. Semliki Forest virus persistence in mouse L929 cells. *Virology* 100:141-155.
18. Robb, J. A., and C. W. Bond. 1979. Coronaviridae, p. 193-247. In H. Fraenkel-Conrat and R. R. Wagner (ed.), *Comprehensive virology*, vol. 14. Plenum Publishing

- Corp., New York.
19. Rottler, P. J. M., W. J. Spaan, M. C. Horzinek, and B. A. M. van der Zeijst. 1981. Translation of three mouse hepatitis virus strain A59 subgenomic RNAs in *Xenopus laevis* oocytes. *J. Virol.* 38:20-26.
20. Sauerbier, W., and K. Hercules. 1978. Gene and transcription unit mapping by radiation effects. *Annu. Rev. Genet.* 12:329-363.
21. Schochetman, G., R. H. Stevens, and R. W. Simpson. 1977. Presence of infectious polyadenylated RNA in the coronavirus avian bronchitis virus. *Virology* 77:772-782.
22. Siddell, S. G., H. Wege, A. Barthel, and V. Ter Meulen. 1980. Coronavirus JHM: cell-free synthesis of structural protein p60. *J. Virol.* 33:10-17.
23. Simmons, D. T., and J. H. Strauss. 1972. Replication of Sindbis virus. II. Multiple forms of double-stranded RNA isolated from infected cells. *J. Mol. Biol.* 71:615-631.
24. Spaan, W. J. M., P. J. M. Rottler, M. C. Horzinek, and B. A. M. van der Zeijst. 1981. Isolation and identification of virus-specific mRNAs in cells infected with mouse hepatitis virus (MHV-A59). *Virology* 108:424-434.
25. Stern, D. F., L. Burgess, and B. M. Sefton. 1982. Structural analysis of virion proteins of the avian coronavirus infectious bronchitis virus. *J. Virol.* 42:208-219.
26. Stern, D. F., and S. I. T. Kennedy. 1980. The coronavirus multiplication strategy. I. Identification and characterization of virus-specified RNA. *J. Virol.* 34:665-674.
27. Stern, D. F., and S. I. T. Kennedy. 1980. Coronavirus multiplication strategy. II. Mapping the avian infectious bronchitis virus intracellular RNA species to the genome. *J. Virol.* 36:440-449.
28. Wege, H., S. Siddell, M. Sturm, and V. Ter Meulen. 1981. Coronavirus JHM: characterization of intracellular viral RNA. *J. Gen. Virol.* 54:213-217.
29. Wengler, G., and A. Wengler. 1976. Localization of the 26S RNA sequence in the viral genome type 42S RNA isolated from SFV-infected cells. *Virology* 73:190-199.
30. Wilhelmson, K. C., J. L. Leibowitz, C. W. Bond, and J. A. Robb. 1981. The replication of murine coronaviruses in enucleated cells. *Virology* 110:225-230.

Synthesis of coronavirus mRNAs:
kinetics of inactivation of infectious
bronchitis virus RNA synthesis by UV light.

Reliable Sources:

- <https://www.cuimc.columbia.edu/news/can-uv-light-fight-spread-influenza>
- https://en.wikipedia.org/wiki/Ultraviolet_germicidal_irradiation
- <https://www.webmd.com/cold-and-flu/news/20180212/can-uv-light-be-used-to-kill-airborne-flu-virus-#1>
- <https://www.ncbi.nlm.nih.gov/pmc/articles/PMC3925713/>
- <https://www.sciencemag.org/news/2018/01/could-ultraviolet-lamps-slow-spread-flu>
- <https://time.com/5142211/uv-light-kills-flu-virus/>
- <https://www.newsweek.com/uv-light-flu-810223>
- <https://www.nature.com/articles/s41598-018-21058-w>

CDC suggests use UV to kill COVID-19

安全 | <https://www.cdc.gov/coronavirus/2019-ncov/hcp/faq.html>



Waste Management QAs

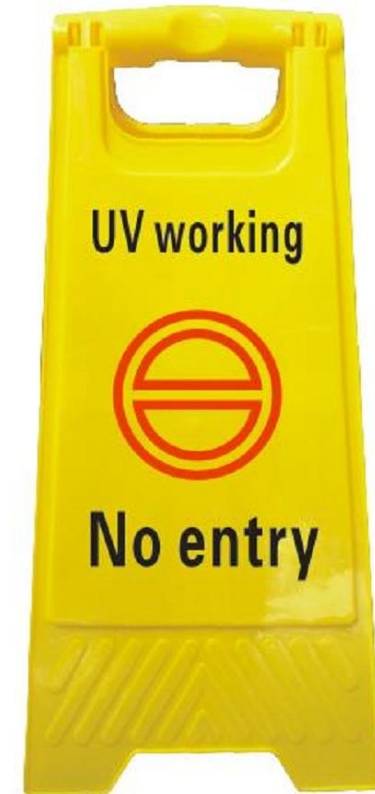
Q: What do waste management companies need to know about wastewater and sewage coming from a healthcare facility or community setting with either a known COVID-19 patient or person under investigation (PUI)?

A: Waste generated in the care of PUIs or patients with confirmed COVID-19 does not present additional considerations for wastewater disinfection in the United States. Coronaviruses are susceptible to the same disinfection conditions in community and healthcare settings as other viruses, so current disinfection conditions in wastewater treatment facilities are expected to be sufficient. This includes conditions for practices such as oxidation with hypochlorite (i.e., chlorine bleach) and peracetic acid, as well as inactivation using UV irradiation.

<https://www.cdc.gov/coronavirus/2019-ncov/hcp/faq.html>

Safety when using UV-C light

While UV-C light is all natural and kills viruses in seconds, human eyes and skin should not be exposed to UV-C light which is invisible. We allow a certain portion of the visible spectrum of light to also be emitted by the device so that the user knows that the UV-C light is active and move away.





A bus is disinfected by ultraviolet light (Picture: China News Service via Getty Images)

Health experts in China are blasting buses with beams of ultraviolet light in a bid to contain the coronavirus outbreak. With viruses spreading via droplets landing on shared surfaces, public transport hubs and vehicles are seen as infection hotbeds. Guidance issued by the National Health Commission says the virus is sensitive to ultraviolet light and heat. Photos taken in Shanghai show entire buses awash with the eerie glow of lamps pumping out beams of radiation to eradicate any trace of the bug.

